International Journal of Heat and Mass Transfer 52 (2009) 4592–4603

Contents lists available at ScienceDirect

International Journal of Heat and Mass Transfer

journal homepage: www.elsevier.com/locate/ijhmt

Heat transfer and pressure drop in furrowed channels with transverse and skewed sinusoidal wavy walls

Shyy Woei Chang [a,1], Arthur William Lees [b,*], Tsu Chien Chou [c,2]

[a] Thermal Fluids Laboratory, National Kaohsiung Marine University, No. 142, Haijhuan Road, Nanzih District, Kaohsiung City, 81143 Taiwan, ROC
[b] School of Engineering, Swansea University, Singleton Park, Swansea, Wales SA2 8PP, UK
[c] Department of Marine Engineering, National Kaohsiung Marine University, No. 142, Haijhuan Road, Nanzih District, Kaohsiung City, 81143 Taiwan, ROC

ARTICLE INFO

Article history:
Received 2 October 2008
Received in revised form 26 February 2009
Accepted 26 February 2009
Available online 4 May 2009

Keywords:
Skewed transverse wavy wall
Furrowed channels

ABSTRACT

This comparative study examines the detailed Nusselt number (Nu) distributions, pressure drop coefficients (f) and thermal performance factors (η) for two furrowed rectangular channels with transverse and skewed sinusoidal wavy walls. Detailed heat transfer measurements over these transverse and skewed sinusoidal wavy walls at the Reynolds numbers (Re) = 1000, 1500, 2000, 5000, 10,000, 15,000, 20,000, 25,000 and 30,000 are performed using the steady-state infrared thermo-graphic method. Impacts of Re on Nu and f for two tested furrowed channels with transverse and skewed waviness are individually examined. In addition to the macroscopic mixing between the near-wall recirculations and core flows due to the shear layer instabilities in each wavy channel, the secondary flows tripped by the skewed wall-waves further elevate heat transfer performances and distinguish their Nu distributions from those over the transverse wavy wall. The area-averaged Nusselt numbers ($\overline{Nu}$) for two tested furrowed channels with transverse and skewed waviness with $5000 < Re < 30000$ fall, respectively, in the ranges of 3.45–3.71 and 3.98–4.2 times of the Dittus–Boelter levels. A set of $\overline{Nu}$ and f correlations for each tested furrowed channel is individually derived using Re as the controlling parameter. By way of comparing the thermal performance factors (η) with a selection of rib-roughened channels, the η factors for the present skewed wavy channel are compatible with those in the channel roughened by the compound V-ribs and deepened scales due to the relative low pressure drop penalties with the equivalent heat transfer augmentations to those offered by V-ribs.

1. Introduction

Wavy channels facilitate considerable heat transfer enhancements (HTE) with relatively low pressure drops in comparison with several different passive enhancement devices such as ribs and vortex generators. Goldstein and Sparrow [1] were among the first to report the existence of longitudinal vortices and the associated heat/mass transfer enhancements in the triangular wavy ducts. Later a number of experimental and numerical studies [2–4], those examined the flow and heat transfer in triangular and corrugated wavy channels, confirmed the almost diminished heat transfer augmentations at relatively low Reynolds numbers ($Re < 1500$) but revealed the evident flow separation, recirculation and reattachment with considerable HTE effects at the higher Re. However, the increases of pressure drops from those in plain ducts were even greater than their heat transfer augmentations [2–4]. In the quest of further reductions in pressure drop penalties, the sinusoidal wavy channels were developed [5–7]. The stable flow recirculation in wavy trough generally developed at low Re. Further increases of Re have led to the interactions of near-wall recirculating flows with the core flows via the shear layer instability [6] and the self-sustained oscillations [4,8–10] that promotes the macroscopic mixings between the near-wall and core fluids. Although the enhanced near-wall to core fluid mixings serve as the primary mechanism for heat transfer augmentations in wavy channels, the corrugated and the convergent–divergent (furrowed) wavy channels give rise to markedly different interactions between recirculation flows and core flows. When the flow moves downstream from the converging part into the diverging part of a furrowed channel, the streamwise adverse pressure gradients causes flow separation with the development of flow reversal in the bulge portion [11]. The trapped vortices almost occupy the entire trough of a furrowed channel. Further downstream from the divergent to convergent cross-sections, the repeated reverse of streamwise pressure gradients triggers flow re-attachments. By way of further increasing Re from laminar to transitional flow in the furrowed

* Corresponding author. Tel.: +44 1792 295837; fax: +44 1792 205678.
E-mail addresses: swchang@mail.nkmu.edu.tw (S.W. Chang), A.W.Lees@swansea.ac.uk (A.W. Lees), tsuchien@hotmail.com (T.C. Chou).
[1] Tel.: +886 7 8100888 5216.
[2] Tel.: +886 7 8100888 5217.

0017-9310/$ - see front matter © 2009 Elsevier Ltd. All rights reserved.
doi:10.1016/j.ijheatmasstransfer.2009.02.039

Nomenclature

a	wave amplitude (m)
d	diameter of the smooth tube (m)
f	pressure drop coefficient = $\Delta P/(0.5\rho W_m^2)(d/4L)$
f_∞	Fanning friction factors in plain tube ($16/Re$ for laminar flow and the Blasius equation of $0.079Re^{-0.25}$ for turbulent flow)
H	channel height (m)
k_f	thermal conductivity of fluid ($Wm^{-1}K^{-1}$)
L	channel length (m)
Nu	local Nusselt number = $q_f d/\{k_f(T_w - T_b)\}$
$\overline{Nu}$	area-averaged Nusselt number over wavy wall
Nu_∞	Nusselt numbers in plain tube (48/11 for laminar flow and Dittus–Boelter correlation for turbulent flow)
ΔP	pressure drop between channel entry and exit (Nm^{-2})
q_f	convective heat flux (Wm^{-2})
Re	Reynolds number = $\rho W_m d/\mu$
T_b	fluid bulk temperature (K)
T_w	wall temperature (K)
W	channel width (m)
W_m	mean flow velocity at entrance of test section (ms^{-1})
X,Y,Z	coordinates (m)

Greek symbols

ρ	density of fluid (kgm^{-3})
μ	fluid dynamic viscosity ($kgm^{-1}s^{-1}$)
λ	wave pitch (m)
η	thermal performance factor = $(Nu/Nu_\infty)/(f/f_\infty)^{1/3}$

channel yields the flow to the unsteady self-sustained oscillatory state. With flow conditions above than the transitional *Re*, the destabilization of the thermal boundary-layer replenishes the near-wall fluid with the core fluid, which in turn augments heat transfer rates. Although the transitional *Re* for the onset of self-sustained oscillations varies with the geometrical factors of a wavy channel, it is typically low enough to be of interest for heat exchangers [9]. In these respects, the onset of wall-to-core mixing is accompanied with the formation of roller vortices in the free shear layer that triggers small oscillations in core flows [10]. Such shear layer driven exchange of fluids results in enhanced macroscopic mixing and introduces three-dimensionality in the flow [10]. For the corrugated channel, the core flow is forced to turn so that the trapped recirculation zone in each wavy trough is smaller than that in the furrowed channel. This results in the macroscopic wall-to-core mixing in the corrugate channel when the core flow undergoes large oscillation at the *Re* above than the transitional *Re* [10], causing considerable changes in the positions of the re-attachment points of the shear layer. When the reattachment point shifts far enough upstream, the core flow injects free-stream fluid into the recirculation cell along with the simultaneous ejection of fluid from the recirculation cell into core flows. Such wall-to-core mixings appear as a dynamic process which has led to considerable heat transfer augmentation.

With turbulent flows in wavy channels, the longitudinal and spanwise vortical flows, which are induced by the waviness of channel-wall, redistribute the turbulent kinetic energy that affects the local velocity gradients of flow and thus the wall shear stresses. Effects of such turbulent interactions on wall shear stresses and on wall heat fluxes are particularly enhanced in the wavy ducts [11]. For turbulent flows in furrowed channels [12], the shear layers promote the production of turbulence, which causes the shrinkage of the separation bubble from that developed for laminar flow in the trough of a wavy wall. Local peaks of Reynolds stresses in the near-wall region are generated near which the separation bubble is initiated. These high Reynolds stresses diminish the thickness of viscous sublayer, thus increasing the gradients of wall temperature, which leads to a local peak in Nusselt number shortly behind the point of separation. In the corrugated rectangular, trapezoidal and triangular ducts, the magnitudes of the secondary flows at their corner regions can reach about 10 times of those in the straight duct with similar cross-sections [11]. Comparative studies between the laminar and turbulent flows in the wavy channels indicated that the secondary flows (laminar case) driven by the sharp corners of the non-circular corrugate ducts were much weaker and different from the turbulence driven secondary flows [11,13]. As an effect of increased shear stresses in the layer which separates the recirculation bubble from the main turbulent flow, the augmented Reynolds stresses result in the higher streamwise velocity gradients at the wall and reduce the size of the recirculation bubble compared to laminar flow; they therefore shorten the axial span of minimum Nusselt numbers (*Nu*) in the bulge of the furrowed channel [12].

Furthermore, the turbulent flow and heat transfer in a wavy channel show different behaviors depending on *Re* and the wave amplitude [14]. The primary source for vortex enhancement in the up-slope region of an undulant wall is identified as the vortex stretching accompanying by the near-wall flow acceleration, together which the vortices are more intensified as the wave amplitude is increased [15]. Therefore, by systematically increasing the wave amplitude, the spatial *Nu* distributions gradually deviate from the sinusoidal pattern developed over the undulant wall with small wave amplitude. With large amplitudes of wall waves, the *Nu* distribution is considerably affected by the appearance of flow separation; the *Nu* peaks develop near the wavy crest where the inviscid free-stream velocity is maximum [14]. The *Nu* values are generally larger in the up-slope part of the undulant wall where the maximum *Nu* and friction coefficient are both developed. In this regard, the peaks of the friction coefficient and *Nu* are, augmented about three and four times by increasing the wave amplitude-to-pitch ratio form 0.01 to 0.1 respectively [15].

In addition to these aforementioned thermal fluid physics in wavy channels, the previous studies [1–16] also examined the influences of shifting phase angle (0°, 90° and 180°) between two opposite wavy walls on flow structures [10], the comparative differences between laminar and turbulent wavy channel flows [12], the impacts of channel cross-sectional shape on fluid flow and heat transfer [11] and the effects of interspacing [2,10,14,16] on the furrowed and corrugate channels. Depending on the interspacing between two opposite wavy walls, two different types of transition to turbulence, namely (1) the instability of the shear layer between main flow and recirculation bubbles in the trough of a wavy wall for a narrow channel and (2) the centrifugal instability on the concave surface leading to Taylor–Goertler vortices with a stable three-dimensional form for channels with large interspacing, are reported [16]. These different instability mechanisms for the wavy ducts with different interspacing can significantly change the vortex wavelength. In general, the larger the interspacing, the smaller the longitudinal vortex diameter or vortex wavelength relative to the interspacing is observed [16]. Recently, a novel measurement technique that spatially resolves and simultaneously detects the turbulent velocity and temperature fields using digital particle image velocimetry (PIV) and liquid crystal thermometry (LCT) was proposed by Philipp Rudolf von Rohr and his

group [17,18]. In a water channel between a sinusoidal heated bottom and a flat top wall, the large-scale longitudinal flow structures carry the bulk of the kinetic energy over the sectional plane parallel to the channel-wall; the low-momentum high-temperature fluid coming from the heated wall replaces the high-momentum low-temperature fluid which convects toward the wall. High-temperature low-momentum flow structures were developed as the fluid is partly decelerated by the wall shear and heated by the hot wall during the streamwise convection. Such thermal structures are observed periodically in the spanwise direction and elongated in the streamwise direction. These transferring mechanisms that convected the near-wall high-temperature fluid to the cold core-region were three-dimensional. Heat transfer enhancements over the wavy wall were the result of complex interactions between the core fluid and the boundary-layer fluid through the shear layer destabilization and self-sustaining oscillations [17]. The follow-up work of this research group [18] examined the mixed convection from a wavy surface at the flow conditions of $1025 < Re < 2102$ and the Grashof numbers in the range of $1.3 - 1.94 \times 10^6$ with the attempt to disclose the influence of mixed convection on turbulence quantities and scalar transport properties. With mixed convection over a wavy wall, a meandering of the scalar plume induced by longitudinal flow structures was observed and led to the spanwise spreading of the mean scalar field. As a result, the spanwise scalar transport such as turbulent heat flux was greatly enhanced by mixing convection compared to the isothermal condition. Due to the enhanced vertical transport driven by buoyancy effects and the enhanced spanwise transport triggered by the mixed convection induced longitudinal flow structures, the momentum transport was increased from the isothermal condition for the mixed convective flow.

With the thermal fluid analysis available to date for wavy channels, the wall-waves are always normal to the main flow [1–18]. No previous attempt examines the heat transfer and pressure drop in a wavy channel with the main flow skewed to the wall-waves. As implied by the skewed ribs which can further enhance heat transfer rates from those augmented by the transverse ribs on the expense of increased pressure drops due to the development of rib-wise secondary flows, this study is motivated to comparatively examine the heat transfer and pressure drop performances in the furrowed channels with transverse and skewed sinusoidal waves. Detailed heat transfer measurements over two wavy walls with transverse and skewed sinusoidal waves are performed using the steady-state infrared thermo-graphic method at $Re = 1000$, 1500, 2000, 5000, 10,000, 15,000, 20,000, 25,000 and 30,000. The spatially averaged Nusselt numbers ($\overline{Nu}$) over each wavy surface, the pressure drop coefficients (f) and the thermal performance factors (η) for two furrowed channels are analyzed with the influence of Re and wave orientation examined. Empirical correlations for $\overline{Nu}$ and f coefficient for two furrowed channels are accordingly derived.

2. Experimental details

2.1. Facilities and test module

The assemblies of the test module with two opposite sinusoidal wavy walls are depicted in Fig. 1. As shown in Fig. 1, the airflow entered the divergent entry plenum chamber (1) in which the meshes and honeycomb were installed. The entry plenum chamber (1) was connected with the Teflon entry flange (2) through which the flow passage at the flange central exactly matched the shape and area of the cross-section of each the furrowed channel with transverse or skewed waviness. Between the entry (2) and exit (3) flanges, a 30 mm thick Teflon wavy back wall (4) was installed. Two sets of 0.1 mm thick stainless steel foils of 54 mm in width (W) and 194 mm in length (L) were forged to form the wavy heating foils (5,6) with transverse or skewed sinusoidal waves. The amplitude (a) and the wave pitch (λ) for each wavy surface were 2.4 mm and 12 mm, respectively, which defined the sinusoidal waviness with the amplitude-to-pitch ratio of 0.2. As the peripheral lengths of each cross-section (S) for the transverse or skewed wavy channels was 135 mm or 174 mm, the hydraulic diameters (d) of these two wavy channels were, 21.6 mm and 16.8 mm respectively and these were selected as the characteristic lengths to evaluate Nu and Re. The wavy heating foil (5) was attached on the wavy back wall (4). Another wavy heating foil (6) was secured in the front Teflon frame (7) to allow the optical assessment of wall temperature (T_w) measurements over this wavy foil. The detailed T_w measurements over the wavy heating foil (6) for each test condition were imaged by a calibrated two-dimensional infrared radiometer (8) which took 0.3 s to complete a 239×255 matrix scan. The back surface of the wavy heating foil (6) was painted black to increase its emission. Each end of the heating foil (5) or (6) was squeezed between the two-piece entry (9) or exit (10) copper plates which were, sandwiched between the flow entry/exit flanges (2,3) and the back/front Teflon walls (4,5). Two Teflon channel sidewalls (11,12) with the waviness to fit the front and back wavy foils (6) set the channel height (H) of 13.5 mm for each wavy channel, which gave the channel aspect ratio (W/H) of 4. The complete electrical circuit for two heating foils of each wavy channel was connected in series by means of two copper plates (8,9) connecting the electrical terminals with the stainless steel heating foils (5,6) and secured on the entry and exit flanges(2,3). The adjustable high-current, low voltage DC power supply connected with the copper plates (8,9) to control the heat fluxes over these heating surfaces. The adjustable and basically uniform heat flux over each wavy stainless steel heating foil was generated. The ranges of heating power and T_w over the wavy heating foil (6) were 62–210 W and 65–120 °C, respectively. A convergent exit plenum chamber (13) was fitted at the exit of each wavy channel. This exit plenum chamber (13) allowed fitting the pressure control valve after the exit of the test section. Components (1–13) were tightened by four draw bolts through four positioning holes on the entry and exit flanges (2,3). The X–Y coordinate system adopted here is also indicated in Fig. 1 with its origin positioned at one lower entry corner of each wavy channel. The test coolant, pressurized air, was fed from an air tank connected with the dehumidifier and the screw-type compressor. Prior to entering the test section, the dry and cooled airflow was channeled through a set of pressure regulator and filtering unit (15), a needle valve (16), a mass flow meter (17) at which the mass flow rate of coolant was adjusted and measured and a digital pressure gauge (18) measuring the entry flow pressure. The dry air is the test fluid for this study.

As depicted in Fig. 1, the two opposite wavy surfaces for each wavy channel were arranged as the in-line manner to form the furrowed channel and characterized by the four dimensionless geometric parameters, namely the channel length (L) to channel width (W) ratio of 194 mm/54 mm = 3.6, the channel width (W) to channel height (H) ratio of 54 mm/13.5 mm = 4, the wave amplitude (a) to channel height (H) ratio of 2.4 mm/13.5 mm = 0.178 and the wave amplitude (a) to pitch (λ) ratio of 2.4 mm/12 mm = 0.2. The angles of attack for the transverse and skewed wavy walls were 90° and 45°, respectively. The comparisons of various Nu distributions between the transverse and skewed wavy channels uncovered the impacts of wave skewness on the heat transfer performances. A K-type thermocouple was positioned at the geometric center of the flow entry section and sandwiched between the entry plenum chamber (1) and the flange (2) to detect the fluid entry temperature. With the similar mechanical layout at the flow exit, three X-wise K-type thermocouples alongside the centerline

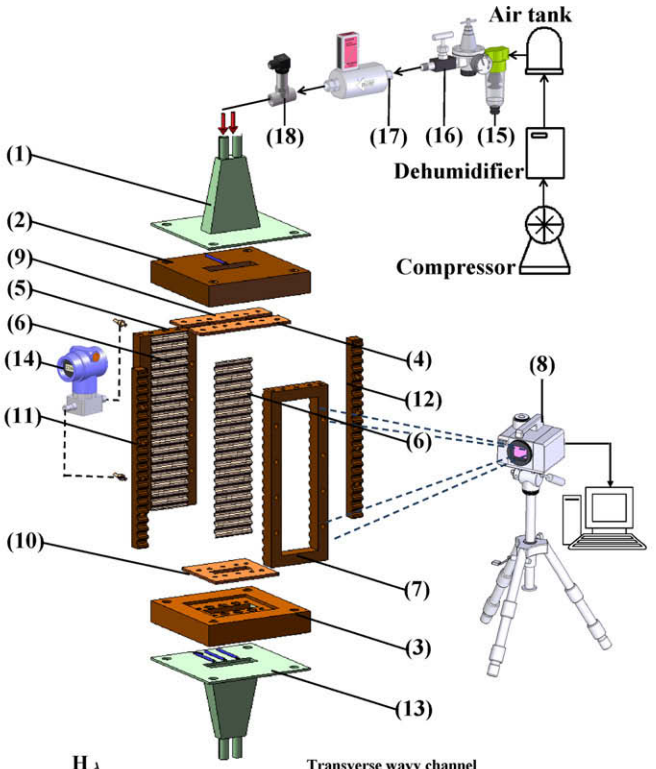

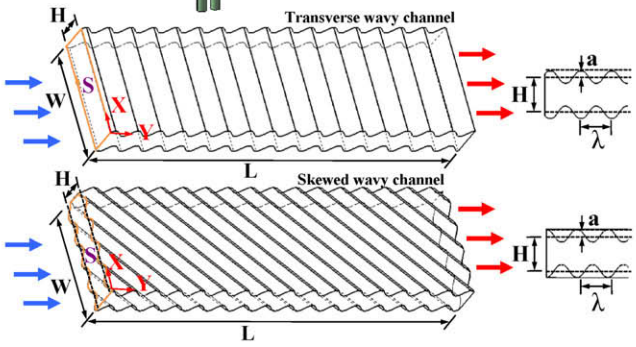

Test channel	W	H	S	λ	a	L	d
Transverse wavy channel	54	13.5	135	12	2.4	194	21.6
Skewed wavy channel	54	13.5	174	12	2.4	194	16.8

Dimension in mm

(1) Entry plenum chamber (2) Entry flange (3) Exit flange
(4) Wavy back wall (5)(6) Wavy heating foils (7) Front frame
(8) Infrared radiometer (9)(10) Entry/exit copper plate (11)(12) Channel sidewall
(13) Exit plenum chamber (14) Micromanometer (15) Pressure regulator
(16) Needle valve (17) Mass flow meter (18) Pressure gauge

Fig. 1. Experimental facilities and test module.

of the flow exit were positioned with equal intervals to measure the fluid exit temperatures. The measured fluid exit temperature was acquired by averaging these three temperatures detected from the thermocouples at the flow exit.

To measure the pressure drops (ΔP) across each wavy channel at each tested *Re*, two pressure taps were installed at the immediately entry and exit of the wavy channel. These two pressure taps connected with the digital micro-manometer (14) with the precision of 0.01 mm H_2O to detect the ΔP values which are converted into the pressure drop coefficients (f). The pressure drops of the transverse and the skewed wavy channels (ΔP) are individually measured at the isothermal conditions for each *Re* tested.

2.2. Program and data processing

This experimental study acquired the detailed wall temperatures over the entire wavy wall with the transverse or the skewed waviness at *Re* = 1000, 1500, 2000, 5000, 10,000, 15,000, 20,000, 25,000 and 30,000. Within the *Re* range tested, various heating powers were selected to raise the maximum T_w on the scanned surfaces at 120 °C. These different heat fluxes varied the fluid bulk temperatures (T_b) along each wavy channel so that the viscosity and density of coolant were accordingly changed. The coolant flow rate was therefore adjusted to compensate the temperature induced variations in fluid properties with the attempt to control *Re* at the flow entrance within ±1% differences from the targeting

value. Such *Re* control was achieved by using an on-line program that calculated the *Re* at the flow entrance in accordance with the measured fluid temperatures and pressures at the entrance of the test section and the mass-flow-rates of the coolant flows.

For this study, the steady-state heat transfer measurements were performed. The steady-state was referred to the condition as the variations of wall temperature at one spot over the heated surface between several successive scans were less than 0.3 °C. In general, after adjusting the flow rate or the heating power, it took about 30–45 min in order to satisfy the steady-state condition. Having reached the steady-state, the thermal image over the scanned wavy heating foil was captured by the on-line infrared thermal–graphic system; which was subsequently converted into a data base of full field wall temperature measurements and transmitted to the computer storage for data processing into local Nusselt numbers (*Nu*). A local *Nu* was calculated using the equation of $Nu = q_f d/\{k_f(T_w - T_b)\}$ in which the local convective heat flux (q_f) was calculated by subtracting the heat-loss flux from the total heat flux supplied to the heating foil. The *Y*-wise T_b variations were determined based on the principal of energy conversion. With each pre-calculated *Y*-wise q_f distribution, the increase of T_b between two successive *Y* locations was evaluated. Starting from the measured fluid entry temperature, the stepwise calculating routine was performed to calculate the T_b values at the *Y* sections where the wall temperatures were detected. For each *Re* tested, the difference between the calculated T_b and the measured fluid temperature at the exit of each test section was controlled to be less than ±10% which was treated as the basic criterion for a set of raw data to be collected. Having determined the T_b distribution along each wavy channel, the variations of the local coolant's thermal conductivity were taken into account by way of expressing k_f as the function of T_b.

A number of calibration runs was undertaken to determine the characteristics of heat-loss flux. With each individual heat-loss calibration run, the flow passage was filled with fiberglass thermal insulating material. With the scanned wall temperatures over the heating foil reaching the steady-state for each heat-loss calibration run, the heat flux supplied into the heating foils was balanced with the heat-loss flux to the surrounding atmosphere through the thermal paths of the conduction via test assemblies and the natural convection over the exposed heating foil. The heat-loss fluxes and the corresponding averaged wall-to-ambient temperature differences were correlated into an equation for evaluating the heat-loss flux. An additional *K*-type thermocouple was used to measure the ambient temperature during all the heat-loss and heat transfer tests. As the T_w distributions over the wavy surface at each tested *Re* were non-uniform, the distributions of wall-to-ambient temperature difference and therefore the heat-loss flux were not uniform, that resulted in the q_f distributions to be not perfectly uniform. A review of the entire q_f distributions showed the maximum non-uniformity of about 9.3%. The basically uniform heat flux heating condition for this class of heat transfer experiments was simulated. With *Nu* distributions over the wavy surfaces determined for all the test scenarios, the subsequent data processing procedures analyzed the heat transfer results in the attempt to derive the empirical correlations for evaluating the area-averaged Nusselt number ($\overline{Nu}$) over two wavy channels using *Re* as the controllable parameter.

The pressure drop coefficient (f) was calculated from the pressure drop (ΔP) across the channel length (L) of each wavy channel with the mean flow entry velocity (W_m) as the reference velocity using the equation of $f = \Delta P/(0.5\rho W_m^2)(d/4L)$ in which ρ was selected as the fluid density at the entrance of each test section. As the HTE effect offered by each wavy channel was expected to be on the expense of the increased pressure drop, the heat transfer augmentations as well as the increased f values for the two tested wavy channels were referenced by levels in the smooth circular tube with fully developed flows. The reference Nusselt number (Nu_∞) and pressure drop coefficient (f_∞) for laminar flows were, respectively, defined as $Nu_\infty = 48/11$ and $f_\infty = 16/Re$; for turbulent airflows, $Nu_\infty = 0.023Re^{0.8}$ and $f_\infty = 0.079/Re^{0.25}$. Having determined the augmentations of heat transfer and pressure drop for each wavy channel at each *Re* tested, the thermal performance factor (η), which is defined as $(Nu/Nu_\infty)/(f/f_\infty)^{1/3}$ to compare the relative heat transfer augmentation to its associated increase in pressure drop at the constant pumping power condition, was subsequently evaluated and compared with the various η values collected from the other heat transfer augmentation devices.

The maximum uncertainties of *Nu*, *f* and *Re* were calculated following the policy of ASME J. Heat Transfer on reporting the uncertainties in experimental measurements and results [19]. The major sources attributing the experimental uncertainties in *Nu* and *f* were the temperature and pressure drop measurements, respectively. In the respects of temperature and pressure drop measurements, our previous repeatability calibration tests for the present infrared thermal image system have indicated the maximum uncertainty of temperature measurements was ±0.7 K [20] and the precision of the present micro-manometer was 0.01 mm H_2O. Depending mainly on the ranges of measurements and the precisions of the instrumentations, the maximum uncertainties of the following devices were estimated as: micro-manometer (0.6%), mass flow meter (0.3%), wattmeter (0.4%) and pressure gauge (5.2%). Based on these estimated constituent uncertainties from the measuring devices, the maximum uncertainties of the derived parameters for the dimensionless groups were derived as: heat flux (1.1%), fluid viscosity (0.29%), fluid thermal conductivity (0.26%) and fluid specific heat (0.02%). With the wall-to-fluid temperature differences and the pressure drops across the tested wavy channels, respectively, fell in the ranges of 40–85 K and 35- to 115-mm H_2O, the maximum uncertainties associated with *Nu*, *f* and *Re* were estimated as 10.9, 3.8 and 3.1%, respectively.

3. Heat transfer results

Fig. 2 collects the *Nu* distributions over the transverse wavy wall of the furrowed channel at all *Re* tested. As shown in Fig. 2, the streamwise as well as spanwise *Nu* variations follow a general pattern shared by all the results obtained with different *Re*, which reflect the flow interactions between the near-wall recirculating flows and the core flows over the transverse wavy wall. Flow recirculations in each bulge of the furrowed channel, which are induced by the upstream flow separation over the convergent throat, have led to a low *Nu* band across the transverse wavy wall in each bulge. In contrast with the low *Nu* region in each bulge, the accelerated flow through the throat along with its downstream flow reattachment tripped by the reverse of streamwise pressure gradients have led to a high *Nu* band across the throttling wave over the transverse wavy wall. Such streamwise bulge-to-throttle *Nu* variations showed by all the plots collected in Fig. 2 with $1000 < Re < 30{,}000$ are accompanied by a general trend of downstream heat transfer elevations. Clearly, the degrees of heat transfer augmentation tripped by these transverse waves are gradually enhanced in the downstream direction toward an asymptotic region where the undulant heat transfer variations oscillate about the same mean *Nu* and reach the so-called repeated fully developed state. In this respect, the channel length or the wave-number required to reach the repeated fully developed region where these transverse waves can deliver their full HTE effects is systematically decreased as *Re* increases. Such upstream movement of the frontier with full HTE effects is clearly visible by sequentially reviewing the individual plots collected in Fig. 2. With $Re > 20{,}000$, the wave

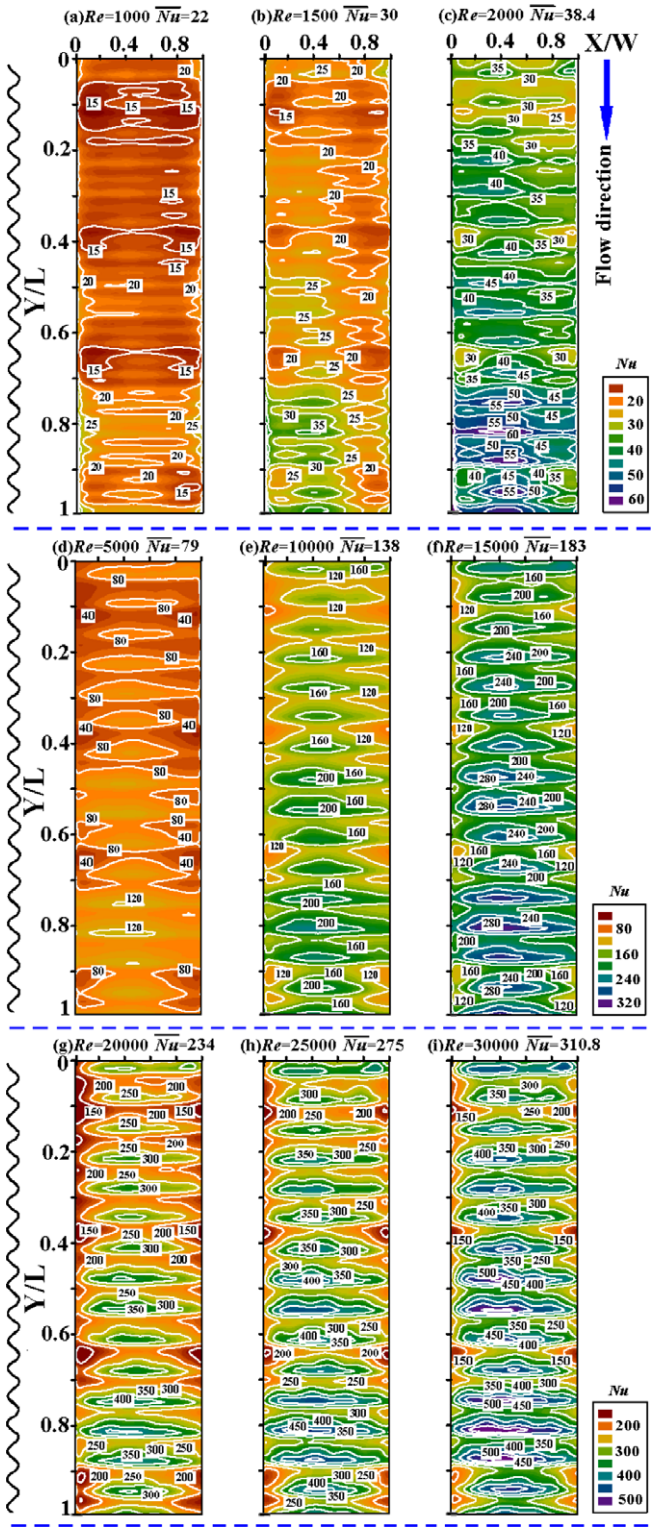

Fig. 2. *Nu* distributions over transverse wavy wall at all *Re* tested.

induced full HTE effects almost occupy the entire channel length as seen in Fig. 2g–i. In view of the *Nu* plots collected from the ascending *Re* in Fig. 2, the developed flow region where the periodical *Nu* variations emerge moves upstream as *Re* increases; while the present wave-numbers are not sufficient to reach the repeated flow region with *Re* < 10,000. In this respect, the previous work [10] also reported that the wavelength at which the flow first became mixed moved upstream as *Re* increased. Eventually, at the high enough *Re*, the demarcation of apparent core-to-wall mixing is initiated at the first wave length [10]. These previous results [10] agree with the present result in the respect of *Re* impact on the developing length for periodical Nu variations. However, although the relatively low *Nu* regions constantly develop in the bulges of the furrowed channel, the heat transfer augmentations from the Nu_∞ references still remain evident. This result suggests that the present *Re* range for this particular channel configuration is higher than the critical *Re* above which the HTE effects are attainable by these transverse waves. Therefore, for the present *Re* range of 1000–30,000, the onset of macroscopic wall-to-core mixing accompanied by the formation of roller vortices in the free shear layer that trigger small oscillations in core flows [10] and the promotion of turbulence productions, which causes the shrinkage of the separation bubble from that developed for laminar flow in the bulge of a wavy wall [12], are likely developed in the present furrowed channel. These flow physics have caused the upstream movement of the frontier with full HTE effects as *Re* increases from 1000 to 30,000 and the considerable *Nu* elevations from the Nu_∞ references.

Another point worth noting heat transfer results implanted in each plot of Fig. 2 is that the symmetrical *Nu* distributions about *X* = 0.5 W centerline. In this respect, *Nu* levels along two side edges of the transverse wavy wall appear to be slightly higher than those over the central region at *Re* = 1000, 1500 and 2000. On the contrary with 5000 < *Re* < 30,000, two relatively low *Nu* regions along the two side edges of the transverse wavy wall are evident. This characteristic *Nu* distribution over the transverse wavy wall can be indicative of the cross-sectional secondary flows induced by these transverse "protruding" throttles which direct the cool coolant from the central core toward two sidewalls at *Re* > 5000. This type of cross-sectional flows incur the symmetrical *X*-wise T_w increases form the central core at *X*=0.5 W toward the two sidewalls at *X*/*W* = 0 and 1. The relatively hot coolant thus flows alongside each channel sidewall that results in the low *Nu* region along each side edge of the transverse wavy wall with 5000 < *Re* < 30,000. Nevertheless, when the traversing flow momentum over these transverse wall-waves remains relatively weak with *Re* < 2000 for this particular channel configuration, the cross-sectional secondary flows can not be well established but the flow separations on the transverse wall-waves interacting with the corner flows along each channel sidewall tends to add the regional HTE effects along two side edges. The regional *Nu* levels along two side edges of the transverse wavy wall at *Re* < 2000 can therefore be slightly higher than those over the central region as seen in Fig. 2a–c. Such *X*-wise heat transfer distributions with the higher *Nu* along two side edges are getting vague as *Re* increases from 1000 to 2000 and reversed to the lower *Nu* along two side edges as *Re* > 5000. In this respect, a more detailed *X*-wise *Nu* variations across the transverse wavy wall will be later examined by sectioning the *Nu* topologies over the transverse wavy wall at several selected *Y*/*L* locations. Future detailed flow measurements are also necessary in order to resolve the flow physics responsible for this particular heat transfer behavior discovered over the present transverse wavy channel.

Fig. 3 collects the *Nu* distributions over the skewed wavy wall of the furrowed channel at all *Re* tested. The streamwise bulge-to-throttle *Nu* variations accompanied by the general trend of downstream heat transfer elevations are still evident in all the plots collected in Fig. 3. But the wave-wise *Nu* variations tripped by the skewed wall-waves consistently show the higher *Nu* along the side edge at *X*/*W* = 1. In this respect, *Nu* levels decay along each skewed wall-wave from the side edge of *X*/*W* = 1 toward another side edge of *X*/*W* = 0. Clearly, the skewed waves have induced the strong cross-sectional secondary flows in the wave-wise direction which interact with the complex wall-to-core mixing to generate the characteristic *Nu* distributing pattern revealed in each plot of

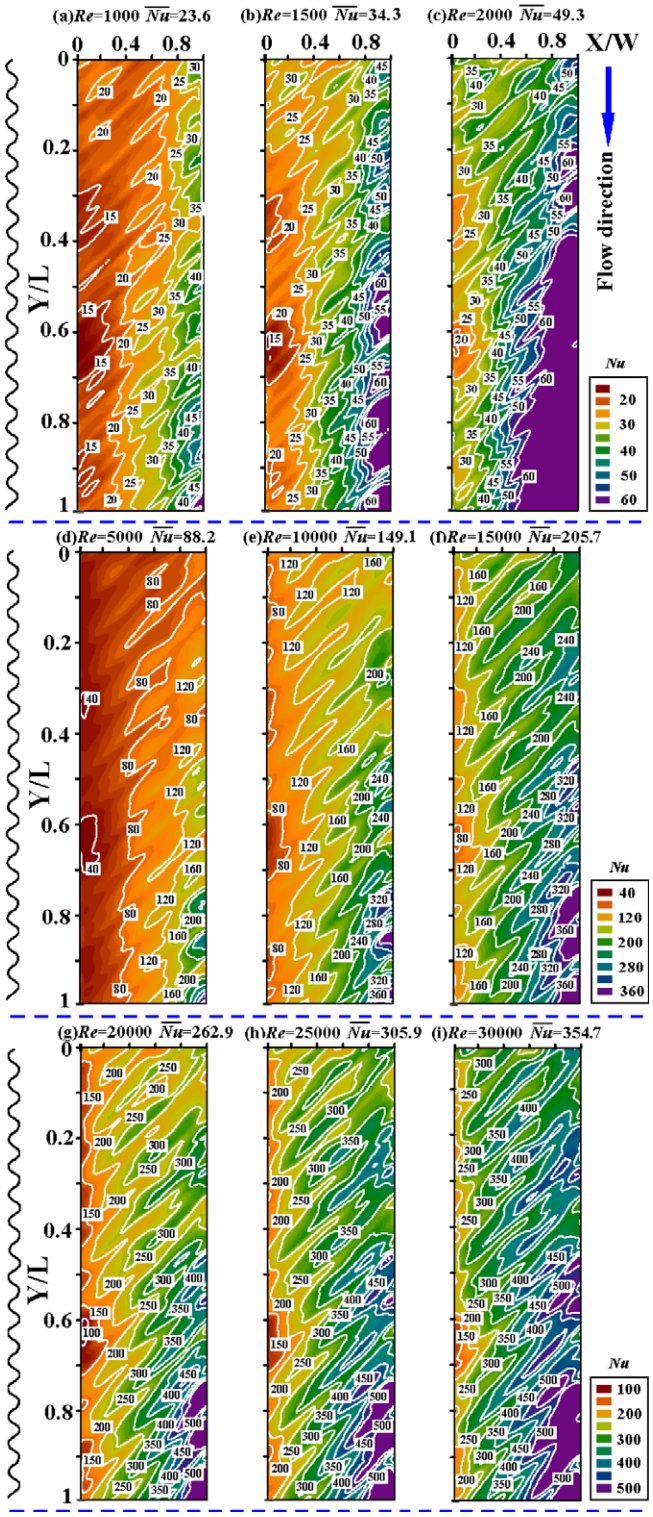

Fig. 3. *Nu* distributions over skewed wavy wall at all *Re* tested.

Fig. 3. These wave-wise secondary flows sweep the recirculating flows in each bulge, swirl the roller vortices in the free shear layer and alter the turbulent interactions, which lead to further augmentations of HTE effects and *f* values. By way of comparing the area-averaged Nusselt number ($\overline{Nu}$) at each *Re* tested over the transverse and skewed wavy walls as cited in Figs. 2 and 3, the $\overline{Nu}$ values in Fig. 3 over the skewed wavy wall are consistently higher than the counterparts indicating in Fig. 2 over the transverse wavy wall. Each plot in Fig. 3 also indicates the general trend of enhancing HTE effects in the downstream direction toward a repeated fully developed region. Again, the developing length or wave-number over the skewed wavy wall systematically decreases as *Re* increases. But, as seen in Fig. 3, the upstream movement of the frontier with the full HTE effects generated by the skewed waves is still persistent up to *Re* = 30,000. At each *Re* tested, the channel length or the wave-number required to reach the repeated fully developed region for the skewed wavy channel is increased from that in the transverse wavy channel due to the development of wave-wise secondary flows.

Fig. 4 compares the detailed *Nu* distributions over a wave pitch between the transverse and skewed wavy channels at *Re* = 30,000. The *Nu* distributions over the pitch of the transverse wavy wall are symmetrical about the channel centerline (*X*/*W* = 0.5). But the *Nu* distributions upstream and downstream of the throat are not symmetrical with the denser *Nu* contours developed on the downstream divergent bulge of the throat where the *Nu* values are generally lower than the counterparts over the upstream converging throttle. Over each pitch of the transverse wavy wall, the *Nu* peak develops at the central locus of the throat. Away from the central *Nu* peak over the transverse wavy wall, the *Nu* levels decay symmetrically toward two sidewalls but asymmetrically toward the upstream divergent-throttle and the downstream convergent-bulge. Over the wave pitch of the skewed wavy wall, the *Nu* decay from the leading edge toward the trailing edge is evident due to the development of strong wave-wise secondary flows. The higher *Nu* values over the skewed wave pitch still develop along the throat with the peak *Nu* at the locus aside the leading edge of the skewed wave pitch. But the decays of *Nu* levels from the *Nu* peak over the skewed wave pitch are both asymmetrically toward two side edges and toward the upstream throttle and the downstream bulge. Unlike the *Nu* distributions over the transverse wavy pitch, the relatively high *Nu* values still prevail along the leading edge of the skewed wave pitch. Cold fronts of the coolant flows tend to initially encounter with the leading edge of each skewed wavy wall prior to washing diagonally along the skewed wave pitch. Therefore, similar to the rectangular channel with two opposite walls roughened by the in-lined 45° ribs, the two-cell cross-sectional secondary flows are tripped by the two opposite skewed throttling waves that initially convect the cold core-fluids toward the leading edge of each skewed wave. The pair of cross-sectional secondary flows washes two opposite heated wavy walls from their leading edges toward the trailing edges after which the confluent fluids swirl to further downstream locations. Accordingly, the local coolant temperatures increase in the diagonal direction along each skewed wave pitch to generate the diagonal decreases of *Nu* in each skewed wave pitch. Similar to the transverse wave pitch, the convergent throttle upstream each diagonal

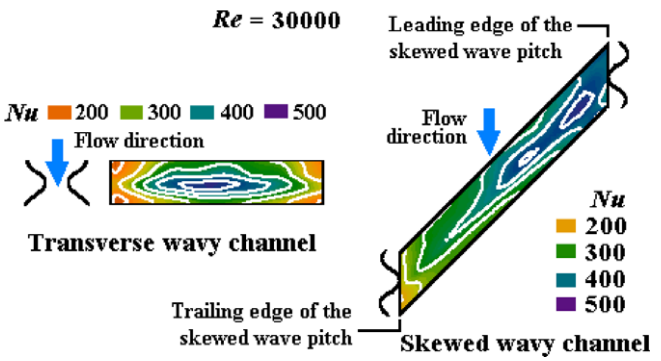

Fig. 4. Detailed *Nu* distributions over a wave pitch of transverse and skewed wavy channels.

throat over the skewed wavy wall possesses the higher Nu than those over the downstream convergent-bulge.

Fig. 5 compares the *X*-wise *Nu* profiles sectioned from the transverse and the skewed wavy walls along *Y*/*L* = (a) 0.25 (b) 0.5 (c) 0.75 for all *Re* tested. At the first glance of Fig. 5, local *Nu* increases as *Re* increases. The increase of *Y*/*L* from 0.25 to 0.75 gradually elevates the overall *Nu* levels in both the transverse and skewed wavy channels. As illustrated previously, the *X*-wise *Nu* variations over the transverse wavy wall are symmetrical; while the skewed *Nu* variations accompanied by the *Nu* bumps at the throats of the

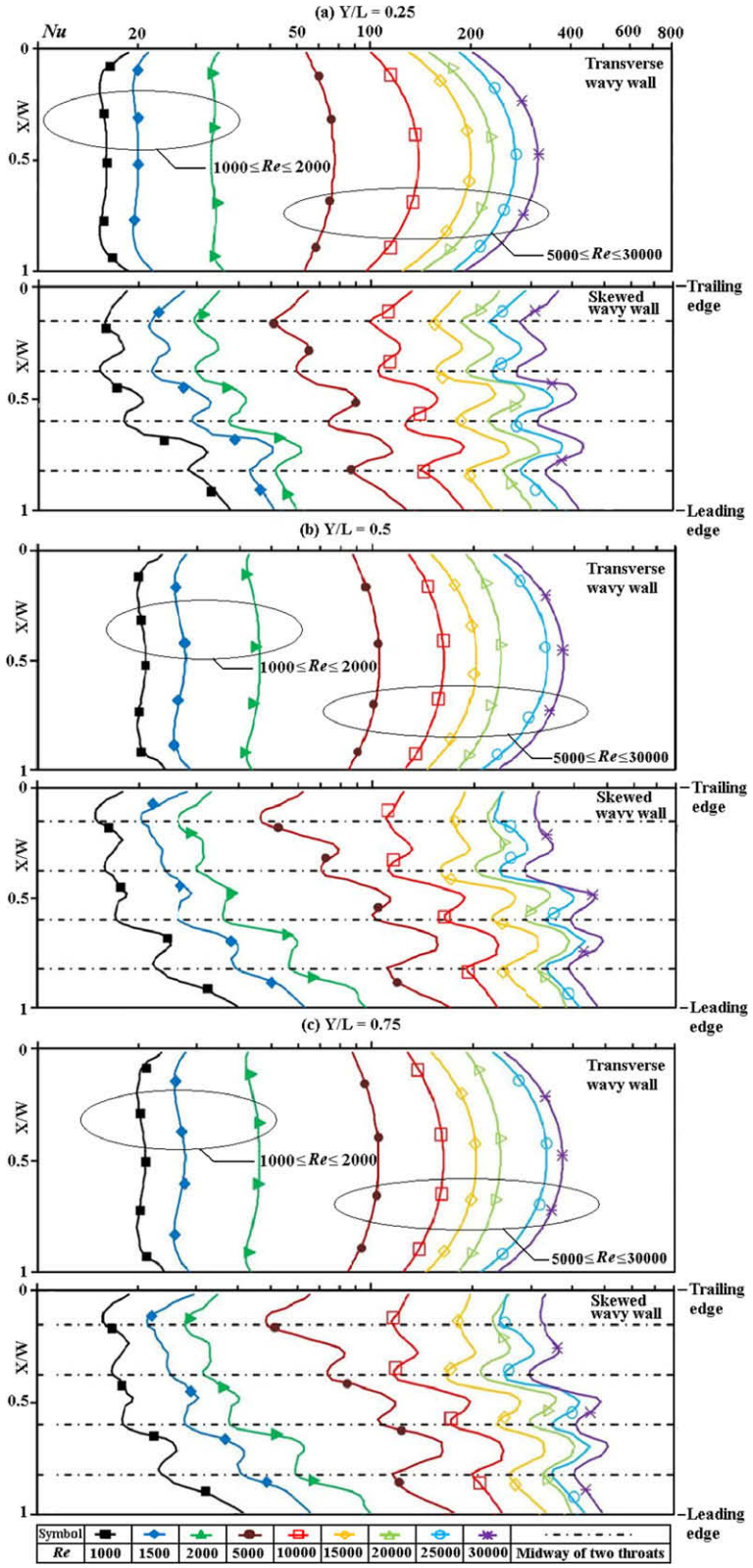

Fig. 5. Comparison of *X*-wise *Nu* profiles between transverse and skewed wavy walls along *Y*/*L* = (a) 0.25 (b) 0.5 (c) 0.75 for all *Re* tested.

furrowed channel with skewed wall-waves consistently show the leading-to-trailing *Nu* decays. As indicated in Fig. 5 for the skewed wavy wall, the regionally minimum *Nu* values constantly develop at the midways between two adjacent throats where the recirculating flow cells are retained within the convergent-bulges. Justified by the evident leading-to-trailing skewness over the skewed wavy wall at all the *Y*/*L* sections in the present *Re* range as depicted in Fig. 5, the 45° inclined wall-waves can trip the strong wave-wise sectional flows even at *Re* = 1000. With the transverse wavy wall, two distinct groups of *Nu* profiles as sorted by 1000 < *Re* < 2000 (laminar flow) and 5000 < *Re* < 30,000 (turbulent flow) in each plot of Fig. 5 are consistently observed. As *Re* increases from 1000 to 30,000, the *X*-wise *Nu* profile systematically yields following the trend to elevate the *Nu* levels over the central region of the transverse wavy wall. The *Nu* elevations over the central region of these transverse waves still remain symmetrical to the streamwise centerline of *X*/*W* = 0.5. Such a varying manner of *X*-wise *Nu* profiles responding to the increase of *Re* from the laminar (*Re* < 2000) to turbulent (5000 < *Re* < 30,000) flow regimes reflects the enhanced heat convection over the central region of each transverse wave due to the enhanced regional core-to-wall macroscopic mixings by the additional turbulence interactions as well as the enhanced wave-wise secondary flows which drive the cold core-coolant from the central region toward two sidewalls alongside each transverse wave. Justified by the two distinct *X*-wise *Nu* patterns collected in Fig. 5 for the laminar (*Re* < 2000) and turbulent flows (5000 < *Re* < 30,000) over the transverse wavy wall, the stronger core-to-wall macroscopic mixings with the higher HTE effects are likely to shift from two side edges with laminar flows toward the wave central for turbulent flows due to the presence of turbulent complexities.

Fig. 6 compares the *Y*-wise (streamwise) *Nu* profiles sectioned from the transverse and the skewed wavy walls along *X*/*W* = (a) 0.25 (b) 0.5 (c) 0.75 for all *Re* tested. In each plot of Fig. 6, local *Nu* valleys and peaks over the transverse or skewed wavy wall, respectively, develop at the midways between two throats and at the throats of each furrowed channel. The amplitudes of *Nu* oscillations tripped by the undulant walls for the two furrowed channels generally increase as *Re* increases. As the flow features tripped by the transverse wall-waves generally remain symmetrical about the *X*-wise centerline (*X*/*W* = 0.5), there are no significant heat transfer differences between the *Y*-wise *Nu* profiles collected along *X*/*W* = 0.25, 0.5 and 0.75 at each *Re* tested. But it is evident that the general slope for each *X*-wise *Nu* profile over the transverse wavy wall reduces gradually as *Re* increases from 1000 to 30,000. Such reducing *X*-wise slopes for the *Nu* profiles over the transverse wavy wall lead to the shorter developing lengths or the smaller wave-numbers for the flows to reach the repeated region at the higher *Re*. But with the skewed wavy channel, the levels and the overall *X*-wise slopes for the *Nu* profiles collected in Fig. 6a (*X*/*W* = 0.25), b (*X*/*W* = 0.5) and c (*X*/*W* = 0.75) are remarkably different due to the development of the strong wave-wise sectional secondary flows. The nearer the leading (trailing) edge, the higher (lower) the *Nu* levels and X-wise slopes are observed over the skewed wavy wall. In particular, while the overall slopes for the *X*-wise *Nu* profiles along the streamwise axis of *X*/*W* = 0.25 shown in Fig. 6a for the skewed wavy channel are rather "flattened" with *Re* > 5000, the climbing feature of the *X*-wise *Nu* profiles along the *X*/*W* = 0.75 axis as seen in Fig. 6c still remain evident over the skewed wavy wall at *Re* = 30,000. In this respect, although the wave-wise flows induced by the skewed wall-waves add the additional HTE effects upon the enhanced macroscopic wall-to-core mixings offered by the undulant surfaces, the developing length or the wave-number required to reach the repeated flow region is extended due to the presence of wave-wise swirling secondary flows in the skewed wavy channel. By way of shifting the flow region from the leading toward the trailing edges of the wavy wall, the differences in the *Nu* levels between the transverse and skewed wavy channels as compared in Fig. 6a–c are systematically increased as a result of the different flow structures between the sectional secondary flows induced by the transverse and skewed wall-waves.

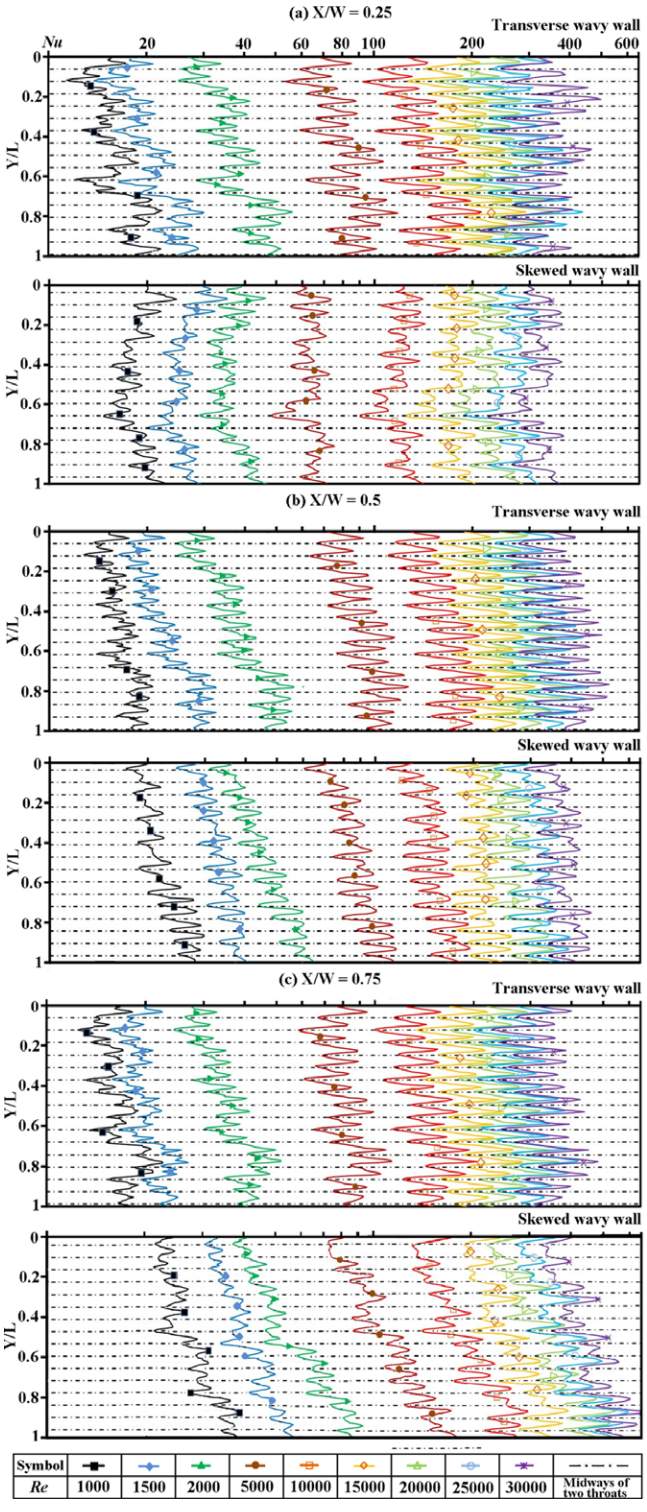

Fig. 6. Comparison of *Y*-wise *Nu* profiles between transverse and skewed wavy walls along *X*/*W* = (a) 0.25 (b) 0.5 (c) 0.75 for all *Re* tested.

The overall heat transfer performances for the two furrowed wavy channels are assessed by comparing the area-averaged

Nusselt numbers ($\overline{Nu}$) over the transverse and skewed wavy walls at each *Re* tested. This is demonstrated in Fig. 7(a) in which the Nu_∞ levels evaluated from the Dittus–Boelter correlation [21] are included to indicate the effectiveness of these wavy walls for turbulent heat transfer augmentation. At each *Re* examined, the skewed wavy channel consistently offers the higher $\overline{Nu}$ than the transverse wavy channel due to the additional HTE effects in association with the secondary flows tripped by the skewed wall-waves. By normalizing $\overline{Nu}$ with Nu_∞ for the laminar and turbulent references, two distinct varying patterns for $\overline{Nu}$ against *Re* as depicted by Fig. 7b are observed. The increase of *Re* elevates the $\overline{Nu}/Nu_\infty$ ratios for laminar flows but reduces the $\overline{Nu}/Nu_\infty$ ratios for turbulent flows. Justified by the continuous $\overline{Nu}$ variations against *Re* as shown in Fig. 7a, the two distinct $\overline{Nu}/Nu_\infty$ versus *Re* patterns between the laminar and turbulent flows in Fig. 7b are caused by the different Nu_∞ references selected for laminar and turbulent flows. The $\overline{Nu}/Nu_\infty$ ratios for laminar flows with $1000 < Re < 2000$ fall between 5.4–11.3 and 5–8.8 for the skewed and transverse wavy channels, respectively. With turbulent flows in the *Re* range of 5000–30,000, the $\overline{Nu}/Nu_\infty$ ratios for the skewed and transverse wavy channels are in the ranges of 4.12–4.03 and 3.8–3.54, respectively. Based on the $\overline{Nu}$ results collected in Fig. 7a, which show that the increase of $\overline{Nu}$ for each tested wavy channel follows a general trend with the limiting condition of diminished forced convective capability ($\overline{Nu} \to 0$) as $Re \to 0$, the $\overline{Nu}$ correlations for the transverse and skewed wavy channels are, respectively, derived as Eqs. (1) and (2).

$$\overline{Nu} = 0.12Re^{0.76} \quad \text{for transverse wavy channel} \tag{1}$$

$$\overline{Nu} = 0.125Re^{0.77} \quad \text{for skewed wavy channel} \tag{2}$$

The maximum discrepancies between the $\overline{Nu}$ values determined by Eqs. (1) and (2) and the experimental data are less than ±15% for the entire $\overline{Nu}$ data generated. For turbulent flows, as the *Re* exponent in the Dittus–Boelter correlation is 0.8, the skewed wavy channel possesses the slightly lesser degree of decaying rates in the $\overline{Nu}/Nu_\infty$ versus *Re* plot because the *Re* exponents in Eqs. (1) and (2) for the transverse and skewed wavy channels are 0.76 and 0.77, respectively. Therefore the effective *Re*-range with HTE effects for the skewed wavy channel is extended from that for the transverse wavy channel.

4. Pressure drops and thermal performance factors

Fig. 8 depicts the variations of (a) pressure drop coefficients (f) and (b) the ratios of f/f_∞ against *Re* for the transverse and skewed wavy channels. As described previously, these f values are evaluated from the pressure drops across the entire length of test channel with the characteristic flow velocity and length scale selected as the mean flow velocity at the entrance and the hydraulic diameter of each test channel, respectively. For each test channel with transverse or wavy walls, the pressure drop coefficients (f) follow the exponential decay as *Re* increases. As compared in Fig. 8-a, the skewed wavy channel consistently operates at the higher f values than those in the transverse wavy channel due to the increased surface areas as well as the strengthened cross-sectional wavewise secondary flows in the skewed wavy channel. As previously described, the HTE benefits from these wall waves are subject to augmentations of f values from the smooth-walled references which are indexed as the ratios of f/f_∞. The comparison of the pressure drop penalties between the transverse and skewed wavy channels is indicated in Fig. 8b by plotting f/f_∞ against *Re* for laminar and turbulent flow regimes. At each tested *Re* for each wavy channel as seen in Fig. 8b, the f/f_∞ ratios are, respectively, increased and reduced for laminar and turbulent flows as *Re* increases systematically. Once again, in view of the continuous f variations against *Re* through the laminar and turbulent flows as shown in Fig. 8a, the two distinct patterns of f/f_∞ versus *Re* depicted in Fig. 8b for laminar and turbulent flows are attributed from the different f_∞ references selected for laminar and turbulent flows. The f/f_∞ ratios for laminar flows with $1000 < Re < 2000$, respectively, fall in the ranges of 4.54–8.63 and 5.36–10.17 for the transverse and skewed wavy channels. With $5000 < Re < 30{,}000$, the f/f_∞ ratios for the transverse and skewed wavy channels are in the ranges of

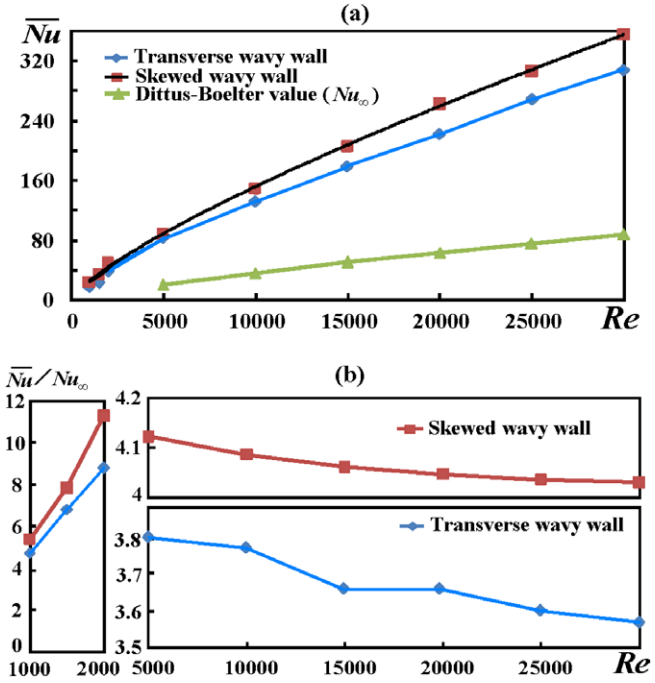

Fig. 7. Variations of (a) $\overline{Nu}$ (b) $\overline{Nu}/Nu_\infty$ against *Re* over transverse and skewed wavy walls.

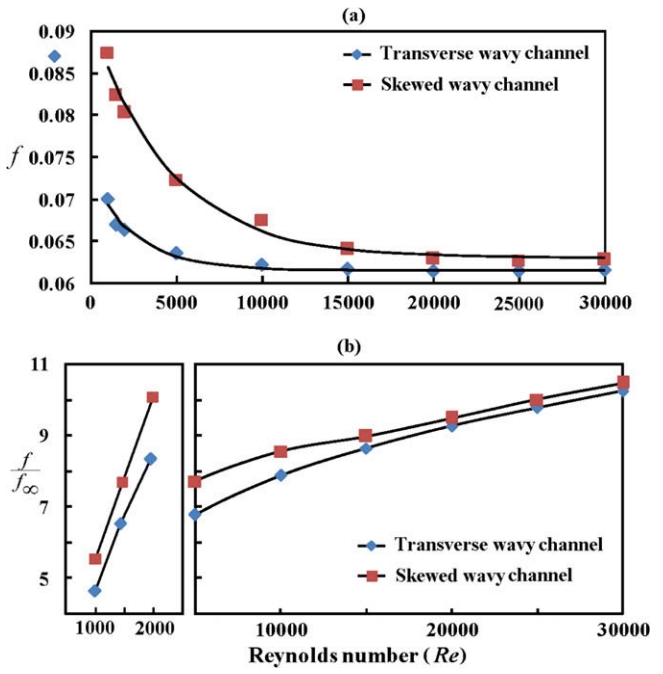

Fig. 8. Variations of (a) f (b) f/f_∞ against *Re* for transverse and skewed wavy channels.

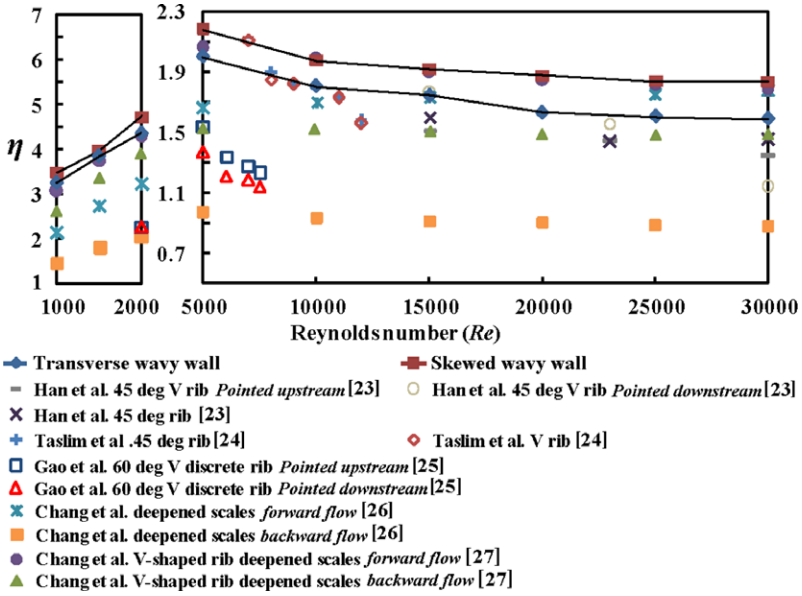

Fig. 9. Comparison of thermal performance factors (η) against *Re* for various HTE surfaces.

5.36–10.17 and 7.72–10.5, respectively. As justified by the data trends depicted in Fig. 8a, the *f* correlations expressed as the function of *Re* for the transverse and skewed wavy channels are, respectively, derived as Eqs. (3) and (4).

$$f = 0.0615 \pm 0.0116 \times e^{-0.000397Re} \quad \text{for transverse wavy channel} \tag{3}$$

$$f = 0.063 \pm 0.0284 \times e^{-0.000219Re} \quad \text{for skewed wavy channel} \tag{4}$$

Maximum discrepancies between the correlated *f* values evaluated from Eqs. (3) and (4) and the experimental data are less than ±10% for the entire *f* data generated.

Having determined $\overline{Nu}/Nu_\infty$ and f/f_∞ ratios for each tested wavy channel with $1000 < Re < 30{,}000$, the assessment of thermal performances for the transverse and skewed wavy channels is performed by comparing their η factors based on the same pumping power consumption. Fig. 9 separately compares the variations of η against *Re* between laminar and turbulent flows for the transverse and skewed wavy channels. Also included in Fig. 9 for comparisons are the η factors in the channels with various HTE surfaces [22–26]. As shown in Fig. 9 as *Re* increases, η factors for both transverse and skewed wavy channels increase for laminar flows but decrease for turbulent flows, which follow the general η versus *Re* trends with the various HTE surfaces [22–26]. In view of the comparative differences between the present transverse and skewed wavy channels, although the transverse wavy channel possesses the lesser degrees of pressure drop penalties, the larger degrees of HTE effects in the skewed wavy channel offset its higher f/f_∞ ratios and result in the higher η factors than those in the transverse wavy channel. In this respect, the η factors fall in the ranges of 3.16–4.33 and 3.34–4.6 for the transverse and skewed wavy channels with laminar flows of $1000 < Re < 2000$, respectively. With $5000 < Re < 30{,}000$, the η factors for the transverse and skewed wavy channels are in the ranges of 1.96–1.59 and 3.5–4.2, respectively. It is worth noting that the η factors for the present skewed wavy channel are compatible with those in the rectangular channel roughened by the compound V-ribs and deepened scales [26] in which the $\overline{Nu}/Nu_\infty$ and f/f_∞ ratios are both higher than those in the skewed wavy channel. For the present skewed wavy channel, the $\overline{Nu}/Nu_\infty$ ratios are among the levels reported for the channels with two opposite walls roughened by V-ribs [22–24] but its f/f_∞ ratios are considerably reduced which together achieve the high η factors compatible with those in the channel roughened by the compound V-ribs and deepened scales [26].

5. Conclusions

This experimental study compares the detailed heat transfer performances for two rectangular furrowed channels with two opposite walls enhanced by a set of transverse or skewed sinusoidal waves with particular emphases on their HTE effects, pressure drops and thermal performance factors. The enhanced macroscopic wall-to-core mixings triggered by the streamwise flow interactions in the form of roller vortices in the shear layer of each furrowed channel tested give the general HTE influences with increased pressure drops. Such streamwise flow interactions with either the transverse or the skewed wall-waves generate the throat-to-bulge *Nu* variations with the regionally maximum and minimum *Nu* developed at throats and bulges, respectively. Additional HTE effects accompanied by the leading-to-trailing *Nu* decays are put forward by the strong wave-wise secondary flows in the skewed wavy channel. Due to the development of wave-wise secondary flows in the skewed wavy channel, the channel length for flows reaching the repeated developed region is extended from that in the transverse wavy channel, although such developing lengths for the transverse and skewed wavy channels are both decreased as *Re* increases. For the transverse and skewed wavy channels, the $\overline{Nu}/Nu_\infty$ ranges fall, respectively, between 5–8.8 and 5.4–11.3 with $1000 < Re < 2000$ and 3.8–3.54 and 4.12–4.03 with $5000 < Re < 30{,}000$. The HTE influences generated by the skewed wall-waves are well-matched with those offered by the V-ribs but are accompanied by the lesser pressure drops so that the thermal performance factors in the skewed wavy channel become compatible with the compound roughness of V-ribs and deepened scales. To assist the design activities using the present transverse or skewed wall-waves for HTE purposes, two sets of $\overline{Nu}$ and *f* correlations with *Re* as the controlling parameter are derived for the present transverse and skewed wavy channels.

References

[1] J.L. Goldstein, E.M. Sparrow, Heat/mass transfer characteristics for flow in a corrugated wall channel, ASME J. Heat Transfer 99 (1977) 187–195.

[2] E.M. Sparrow, J.W. Comb, Effect of interwall spacing and fluid flow inlet conditions on a corrugated-wall heat exchanger, Int. J. Heat Mass Transfer 26 (1983) 993–1005.
[3] Y. Asako, M. Faghri, Finite-volume solutions for laminar flow and heat transfer in a corrugated duct, ASME J. Heat Transfer 109 (1987) 627–634.
[4] M. Ali, S. Ramadhyani, Experiments on convective heat transfer in corrugated channels, Exp. Heat Transfer 5 (1992) 175–193.
[5] T. Nishimura, Y. Kajimoto, A. Tarumoto, Y. Kawamura, Flow structure and mass transfer for a wavy channel in transitional flow regime, J. Chem. Eng. Japan 19 (1986) 449–455.
[6] T. Nishimura, T. Yoshino, Y. Kawamura, Instability of flow in a sinusoidal wavy channel with narrow spacing, J. Chem. Eng. Japan 20 (1987) 102–104.
[7] Y. Asako, H. Nakamura, M. Faghri, Heat transfer and pressure drop characteristics in a corrugated duct with rounded corners, Int. J. Heat Mass Transfer 31 (1988) 1237–1245.
[8] T. Nishimura, A. Tarumoto, Y. Kawamura, Flow and mass transfer characteristics in wavy channels for oscillatory flow, Int. J. Heat Mass Transfer 31 (1987) 1007–1015.
[9] G. Wang, S.P. Vanka, Convective heat transfer in periodic wavy passages, Int. J. Heat Mass Transfer 38 (1995) 3219–3230.
[10] T.A. Rush, T.A. Newell, A.M. Jacobi, An experimental study of flow and heat transfer in sinusoidal wavy passages, Int. J. Heat Mass Transfer 42 (1999) 1541–1553.
[11] M. Rokni, T.B. Gatski, Predicting turbulent convective heat transfer in fully developed duct flows, Int. J. Heat Fluid Flow 22 (2001) 381–392.
[12] G. Russ, H. Beer, Heat transfer and flow field in a pipe with sinusoidal wavy surface – I. Numerical investigation, Int. J. Heat Mass Transfer 40 (1997) 1061–1070.
[13] M. Ronki, B. Sundén, 3D numerical investigation of turbulent forced convection in wavy ducts with trapezoidal cross-section, Numer. Method Heat Fluid Flow 8 (1998) 118–141.
[14] T.S. Park, H.S. Choi, K. Suzuki, Nonlinear k–ε–f_μ model and its application to the flow and heat transfer in a channel having one undulant wall, Int. J. Heat Mass Transfer 47 (2004) 2403–2415.
[15] H.S. Choi, K. Suzuki, Large eddy simulation of turbulent flow and heat transfer in a channel with one wavy wall, Int. J. Heat Fluid Flow 26 (2005) 681–694.
[16] P. Gschwind, A. Regele, V. Kottke, Sinusoidal wavy channels with Taylor–Goertler vortices, Exp. Thermal Fluid Sci. 11 (1995) 270–275.
[17] N. Kruse, Philipp Rudolf von Rohr, Structure of turbulent heat flux in a flow over a heated wavy wall, Int. J. Heat Mass Transfer 49 (2006) 3514–3529.
[18] S. Kuhn, Philipp Rudolf von Rohr, Experimental investigation of mixed convective flow over a wavy wall, Int. J. Heat Fluid Flow 29 (2008) 94–106.
[19] Editorial Board of ASME Journal of Heat Transfer, Journal of heat transfer policy on reporting uncertainties in experimental measurements and results, ASME J. Heat Transfer 115 (1993) 5–6.
[20] S.W. Chang, L.M. Su, T.L. Yang, S.F. Chiou, Enhanced heat transfer of forced convective fin flow with transverse ribs, Int. J. Thermal Sci. 43 (2004) 185–200.
[21] F.W. Dittus, L.M.K. Boelter, Publications in Engineering, vol. 2, University of California, Berkeley, CA, 1930. p. 443.
[22] J.C. Han, Y.M. Zhnag, C.P. Lee, Augmented heat transfer in square channels with parallel, crossed, and V-shaped angled ribs, ASME J. Turbomachinery 113 (1991) 590–597.
[23] M.E. Taslim, T. Li, D. Kercher, Experimental heat transfer and friction in channels roughened with angle V-shaped and discrete ribs on two opposite walls, ASME J. Turbomachinery 118 (1996) 20–28.
[24] X. Gao, B. Sundén, PIV measurement of the flow field in rectangular ducts with 60° parallel, crossed and V-shaped ribs, Exp. Thermal Fluid Sci. 28 (2004) 639–653.
[25] S.W. Chang, T.-M. Liou, M.H. Lu, Heat transfer of rectangular narrow channel with two opposite scale-roughened walls, Int. J. Heat Mass Transfer 48 (2005) 3921–3931.
[26] S.W. Chang, T.-M. Liou, K.F. Chiang, G.F. Hong, Heat transfer and pressure drop in rectangular channel with compound roughness of V-shaped ribs and deepened scales, Int. J. Heat Mass Transfer 51 (2008) 457–468.